



HAL
open science

Upscaling and prediction of Lagrangian velocity dynamics in heterogeneous porous media

Vivien Hakoun, Alessandro Comolli, Marco Dentz

► **To cite this version:**

Vivien Hakoun, Alessandro Comolli, Marco Dentz. Upscaling and prediction of Lagrangian velocity dynamics in heterogeneous porous media. *Water Resources Research*, 2019, 10.1029/2018WR023810 . hal-02471106

HAL Id: hal-02471106

<https://brgm.hal.science/hal-02471106>

Submitted on 7 Feb 2020

HAL is a multi-disciplinary open access archive for the deposit and dissemination of scientific research documents, whether they are published or not. The documents may come from teaching and research institutions in France or abroad, or from public or private research centers.

L'archive ouverte pluridisciplinaire **HAL**, est destinée au dépôt et à la diffusion de documents scientifiques de niveau recherche, publiés ou non, émanant des établissements d'enseignement et de recherche français ou étrangers, des laboratoires publics ou privés.

Upscaling and prediction of Lagrangian velocity dynamics in heterogeneous porous media¹

Vivien Hakoun¹, Alessandro Comoli¹, and Marco Dentz¹

¹Institute of Environmental Assessment and Water Research (IDAEA), Spanish Council of Scientific Research (CSIC), Barcelona, Spain

Key Points:

- Darcy-scale Lagrangian velocities intermittent in travel time, non-intermittent in travel distance
- Lagrangian velocity statistics evolve in time and distance dependent on injection conditions
- Full evolution captured by stochastic relaxation process for equidistantly sampled Lagrangian velocities

¹Hakoun, V., A. Comoli, and M. Dentz, Upscaling and prediction of Lagrangian velocity dynamics in heterogeneous porous media, *Water Resour. Res.*, <https://doi.org/10.1029/2018WR023810>, 2019.

Corresponding author: Marco Dentz, marco.dentz@csic.es

Abstract

The understanding of the dynamics of Lagrangian velocities is key for the understanding and upscaling of solute transport in heterogeneous porous media. The prediction of large scale particle motion in a stochastic framework implies identifying the relation between the Lagrangian velocity statistics and the statistical characteristics of the Eulerian flow field and the hydraulic medium properties. In this paper, we approach both challenges from a numerical and theoretical point of view. Direct numerical simulations of Darcy-scale flow and particle motion give detailed information on the evolution of the statistics of particle velocities both as a function of travel time and distance along streamlines. Both statistics evolve from a given initial distribution to different steady state distributions, which are related to the Eulerian velocity PDF. Furthermore, we find that Lagrangian velocities measured isochronally as a function of travel time show intermittency dominated by low velocities, which is removed when measured equidistantly as a function of travel distance. This observation gives insight into the stochastic dynamics of the particle velocity series. As the equidistant particle velocities show a regular random pattern that fluctuates on a characteristic length scale, it is represented by two stationary Markov processes, which are parametrized by the distribution of flow velocities and a correlation distance. The velocity Markov models capture the evolution of the Lagrangian velocity statistics in terms of the Eulerian flow properties and a characteristics length scale, and shed light on the role of the initial conditions and flow statistics on large scale particle motion.

1 Introduction

The sound understanding of flow and transport processes in heterogeneous porous media is a key requirement for a broad range of applications. This includes the geological storage of nuclear waste [De Marsily *et al.*, 1977; Poinssot and Geckeis, 2012], the sequestration of carbon dioxide in deep saline aquifers [Niemi *et al.*, 2017], aquifer remediation and the management of groundwater resources [Freeze and Cherry, 1979; Domenico and Schwartz, 1997], among others. Flow and transport in groundwater are dominated by spatial heterogeneity in the hydraulic medium properties, which may vary in natural media over more than 12 orders of magnitude [Bear, 1972; Sanchez-Vila *et al.*, 2006]. The impact of spatial variability in the hydraulic conductivity $K(\mathbf{x})$ on the groundwater flow and transport properties have been quantified by stochastic modeling [Rubin, 2003]. In this framework, $K(\mathbf{x})$ is modeled as a random space function [Dagan, 1989; Gelhar, 1993]. The stochasticity of $K(\mathbf{x})$ is mapped onto the flow field $\mathbf{q}(\mathbf{x})$ via the Darcy equation [Bear, 1972]. Stochastic perturbation theory expresses the spatially variable flow velocity as a linear functional of log-hydraulic conductivity $Y(\mathbf{x}) = \ln K(\mathbf{x})$ and upscales solute dispersion by the longitudinal macrodispersion coefficient [Gelhar and Axness, 1983]

$$D_L^* = \sigma_Y^2 \lambda \bar{u}. \quad (1)$$

It is fully characterized by the correlation scale and variance of log-hydraulic conductivity, λ and σ_Y^2 , respectively, and the mean flow velocity \bar{u} . This is a key result of stochastic hydrology because it predicts a transport attribute, macrodispersion, based on independently measurable medium and flow properties. Its limitations are on one hand the fact that it is based on first order perturbation theory in σ_Y^2 and on the other hand that it is only valid at asymptotically long times, this means at times much larger than the advection time scale $\tau_u = \lambda/\bar{u}$. The representation of the impact of velocity fluctuations on large scale transport in terms of constant macrodispersion coefficients is called the macrodispersion approach in the following.

In fact, field and laboratory experiments, direct numerical simulations and theoretical works [Rehfeldt *et al.*, 1992; Zhang, 1997; Sidle *et al.*, 1998; Levy and Berkowitz, 2003; Fiori *et al.*, 2003; de Dreuzy *et al.*, 2007a; Beaudoin and de Dreuzy, 2013] have shown

that asymptotic dispersion coefficients in highly heterogeneous media vary non-linearly with σ_Y^2 . Moreover, preasymptotic transport cannot be described by macrodispersion theory, this means in terms of the advection-dispersion equation characterized by the average flow velocity and constant macrodispersion coefficients. Signatures of pre-asymptotic or non-Fickian transport observed in field and laboratory experiments are, for example, the nonlinear temporal growth of solute dispersion and early and late solute arrivals. Non-Fickian or anomalous behaviors have been modeled by a series of different approaches. Stochastic averaging of the local scale advection-dispersion equation leads to spatio-temporally non-local equations for the average concentration [Neuman and Zhang, 1990; Cushman et al., 1994, 2002; Neuman and Tartakovsky, 2009]. These approaches require a closure approximation for the space-time memory kernels. Space and time fractional advection-dispersion equations [Benson et al., 2000; Cushman and Ginn, 2000; Schumer et al., 2003] model the impact of heterogeneity on transport by memory kernels, which decays algebraically at long distances or at long times. Phenomenologically, these approaches account for strong spatial correlations (space-fractional) and long mass transfer times (time-fractional). The latter is related to the multi-rate mass transfer Haggerty and Gorelick [1995]; Carrera et al. [1998]; Schumer et al. [2003] and continuous time random walk (CTRW) [Berkowitz and Scher, 1997; Berkowitz et al., 2006; Dentz and Berkowitz, 2003] and time-domain random walk (TDRW) approaches [Painter and Cvetkovic, 2005; Cvetkovic et al., 2014], which model anomalous transport through broad distribution of mass transfer times.

For advection-dominated scenarios as typically encountered in heterogeneous porous media, transport can be understood by considering the statistical properties of the Lagrangian velocity [Dagan, 1989], which describes the flow velocity at the position of a particle. In fact, the macrodispersion coefficient can be expressed in terms of the Lagrangian velocity covariance function [Kubo et al., 1991; Dagan, 1989]. Classical random walk approaches model particle velocities as Markov processes in time [Pope, 2000]. The macrodispersion approach, for example, models the fluctuations of particle velocities as a Gaussian noise with zero mean and variance proportional to D_L^* . Thus, the result (1) can be understood as the link between Lagrangian particle dynamics and medium and Eulerian flow properties. Meyer and Tchelepi [2010] have shown that the evolution of Lagrangian velocities may also be modeled as a Markov process in time whose evolution follows a non-linear Langevin equation. The CTRW and TDRW frameworks model non-Fickian solute transport through broad distributions of independent advective transition times over given length scales intrinsic to the medium structure [Berkowitz and Scher, 1997; Painter and Cvetkovic, 2005; Comolli and Dentz, 2017]. In this sense, these approaches assume that particle velocities form Markov processes when sampled equidistantly along trajectories [Cvetkovic et al., 1996; Benke and Painter, 2003; Fiori et al., 2006; Le Borgne et al., 2007, 2008a], this means at time points that are spaced by the advective transition time over a given distance [Cvetkovic et al., 1996; Le Borgne et al., 2007]. It has been shown for heterogeneous porous and fractured media [Painter and Cvetkovic, 2005; Fiori et al., 2007; Le Borgne et al., 2008a; Kang et al., 2011; Ederly et al., 2014; Kang et al., 2017] that large scale particle motion can be modeled by CTRW and TDRW approaches.

For pore-scale particle motion, it has been shown that spatial persistence of flow velocities leads to intermittent patterns in Lagrangian velocity time series [De Anna et al., 2013; Kang et al., 2014; Morales et al., 2017]. This can be traced back to long residence times in regions of low and fast crossing of regions of high flow velocity. We expect to observe similar behaviors for particle velocities in Darcy scale heterogeneous porous media. Intermittency in particle velocities indicates strong correlation of low particle velocities and thus long residence times, which is directly related to the occurrence of anomalous or non-Fickian transport.

Furthermore, several authors [Cvetkovic et al., 1996; Demmy et al., 1999; Le Borgne et al., 2007; Hyman et al., 2015; Dagan, 2017; Kang et al., 2017; Morales et al., 2017] have observed for heterogeneous porous and fractured media, that the Lagrangian ve-

locity statistics and transport characteristics such as breakthrough curves, the center of mass velocity and dispersion of a solute plume are dependent on the distribution of initial particle velocities and thus injection conditions and heterogeneity distribution in the injection region. Thus, a predictive model for particle motion in heterogeneous porous media should be able to account for the impact of different injection conditions on the evolution of particle velocities [Dentz *et al.*, 2016].

The medium heterogeneity acts on the flow field, the flow field on the particle velocities and the particle velocities determine the transport behavior. Thus, a key to understanding transport in heterogeneous media is the understanding of the dynamics of particle velocities. As pointed out above, for weakly heterogeneous media and times much larger than the advection time scale τ_u , velocity fluctuations may be characterized as a white noise characterized by macrodispersion coefficients. In this spirit, the objectives of this study are to identify the dynamics of Lagrangian velocities for strongly heterogeneous porous media, link them to the Eulerian flow statistics and ideally to the statistical medium properties, and quantify their evolution in terms of a predictive upscaled model. To this end, we performed extensive numerical simulations of flow and particle transport in highly heterogeneous porous media. We analyze Lagrangian velocity series sampled both isochronally and equidistantly along streamlines and study the evolution of their probability density functions for different injection conditions. These dynamics are quantified in a predictive analytical Markov model for the equidistantly sampled particle velocities. We consider 2-dimensional heterogeneous porous media. However, the fundamental features of the evolution of Lagrangian velocities are expected to be the same for 3-dimensional media as detailed below.

The paper is organized as follows. Section 2 presents the flow and transport model, defines the velocity statistics for streamwise isochrone and equidistant sampling and the numerical methodology. Section 3 analyzes the evolution of the Lagrangian velocity statistics both in time and streamline distance. Section 4 discusses two analytical Markov models to predict the evolution of equidistant Lagrangian velocities. Section 5 studies the relation between the hydraulic conductivity and the velocity statistics.

2 Flow and transport in heterogeneous porous media

We first present the Darcy scale flow problem and its stochastic description for heterogeneous porous media. Then, we consider the equations of motion of particles in the heterogeneous Darcy flow and formulate the evolution of the particle position in time and in distance along streamlines. The latter is the basis for the definition of the statistics of the velocity magnitude through isochrone and equidistant sampling and relating the Eulerian and Lagrangian velocity statistics. The presented definitions, derivations and relations are valid for 2- and 3-dimensional heterogeneous porous media. Finally we provide details on the numerical simulation method, this means, generation of the hydraulic conductivity $K(\mathbf{x})$ as a random space function with given statistical properties, and the numerical solution of flow and particle motion via particle tracking.

2.1 Flow and Eulerian velocity distribution

Groundwater flow through porous media follows the Darcy equation [Darcy, 1856; De Marsily, 1986]:

$$\mathbf{q}(\mathbf{x}) = -K(\mathbf{x}) \nabla h(\mathbf{x}), \quad (2)$$

where $\mathbf{q}(\mathbf{x})$ is the Darcy velocity, \mathbf{x} is a vector of space coordinates, $h(\mathbf{x})$ is hydraulic head and $K(\mathbf{x})$ is the spatially variable hydraulic conductivity. We consider incompressibility of fluid and medium, this means $\nabla \cdot \mathbf{q}(\mathbf{x}) = 0$. Hydraulic conductivity is modeled as a random space function whose statistics are based on the stationary and ergodic multi-Gaussian random field $Y(\mathbf{x})$, which is fully characterized by its mean $\mu_Y = \langle Y(\mathbf{x}) \rangle$ and

covariance function $C_Y(\mathbf{x}-\mathbf{x}') = \langle Y'(\mathbf{x})Y'(\mathbf{x}') \rangle$ with $Y'(\mathbf{x}) = Y(\mathbf{x}) - \langle Y(\mathbf{x}) \rangle$. The angular brackets denote the ensemble average over all realizations of $Y(\mathbf{x})$. Since $Y(\mathbf{x})$ is ergodic, ensemble and spatial averages are equivalent. We consider here the exponential covariance model

$$C_Y(\mathbf{x}) = \sigma_Y^2 \exp(-|\mathbf{x}|/\lambda), \quad (3)$$

where σ_Y^2 is the variance of the log-hydraulic conductivity, and λ is the correlation length. Hydraulic conductivity is obtained by the map $K(\mathbf{x}) = F[Y(\mathbf{x})]$. For example, for $F(y) = \exp(y)$, $K(\mathbf{x})$ has a Lognormal point-wise probability density function (PDF) $p_K(k)$. *Matheron* [1967] showed that for a K field with Lognormal distribution, the effective hydraulic conductivity K_e is equal to the geometric mean conductivity, $K_e = K_G$. For natural aquifers, the variance of Lognormal K fields has been found in the 0.1–5 range [*Gelhar*, 1993]. For example *Rehfeldt et al.* [1992] report $\sigma_Y^2 \approx 4.5$ for the Columbus aquifer. Variations as high as 10–15 were reported by *Fogg* [2010].

The Lognormal distribution of K has been challenged for heterogeneous sedimentary formations [*Painter*, 1996; *Sanchez-Vila et al.*, 2006; *Haslauer et al.*, 2012]. Moreover, compared to other distributions, the Lognormal has the property that its mean and variance can be adjusted independently. Thus, we consider in this paper a Lognormal distribution of point-wise conductivity values and the truncated Gamma-distribution

$$p_K(k) = N \frac{\beta^\alpha}{\Gamma(\alpha)} k^{\alpha-1} \exp\left(-\frac{k}{k_c} - \frac{k_0}{k}\right), \quad (4)$$

where the shape parameter $\alpha > 0$, k_0 is the lower and k_c the upper cut-off, N is the normalization constant. In the following, we will refer to the Lognormal-distributed conductivity fields as Lognormal fields and the truncated Gamma-distributed as Gamma fields.

In order to compare the degree of heterogeneity of these two distributions, we consider in the following the variance of the logarithm $f(\mathbf{x}) = \ln K(\mathbf{x})$ of the hydraulic conductivity, which is denoted by σ_f^2 . The mean value of $f(\mathbf{x})$ is denoted by μ_f . For the Lognormal fields $f(\mathbf{x}) = Y(\mathbf{x})$. In the following, we consider values of σ_f^2 between 10^{-1} and 12.

The flow velocity $\mathbf{q}(\mathbf{x})$ may be characterized statistically by the Eulerian velocity distribution. Local backward flow may occur due to contrasting adjacent K values, for instance in very heterogeneous K fields, thus giving rise to negative streamwise flow components. Here, we focus on the magnitude of Eulerian velocities, $v_e(\mathbf{x}) = |\mathbf{q}(\mathbf{x})|$. In the following, we refer to velocity magnitudes also in short as velocities. The PDF of Eulerian velocities is defined through spatial sampling as

$$p_e(v) = \lim_{V \rightarrow \infty} \frac{1}{V} \int_{\Omega} d\mathbf{x} \delta[v - v_e(\mathbf{x})], \quad (5)$$

where Ω is the sampling domain and V is its volume. As outlined above, due to ergodicity, spatial and ensemble sampling are equivalent.

2.2 Particle motion and Lagrangian velocities

We consider purely advective transport. The trajectory $\mathbf{x}(t, \mathbf{a})$ of a particle starting at $\mathbf{x}(t=0, \mathbf{a}) = \mathbf{a}$ is described by the advection equation

$$\frac{d\mathbf{x}(t, \mathbf{a})}{dt} = \mathbf{v}_t(t, \mathbf{a}), \quad (6)$$

where $\mathbf{v}_t(t, \mathbf{a}) = \mathbf{q}[\mathbf{x}(t, \mathbf{a})]/\phi$ denotes the Lagrangian particle velocity, ϕ is porosity, which here is assumed to be constant. In the following, we refer to $\mathbf{v}_t(t, \mathbf{a})$ as t(ime)-Lagrangian

velocity because it varies with travel time. Furthermore, we set $\phi = 1$, which is equivalent to rescaling time. The distribution of initial particle positions is denoted by $\rho(\mathbf{a})$.

Taylor [1921] studied t-Lagrangian velocity series in order to quantify tracer dispersion by turbulent motion. Later, *Lumley* [1962] introduced a detailed analysis of Eulerian and t-Lagrangian velocity statistics. In the context of porous media, *Dagan* [1984] analyzed t-Lagrangian velocities for solute dispersion in groundwater flow. As shown in Figure 1, for steady flows through heterogeneous media, the t-Lagrangian velocity series exhibit intermittent patterns characterized by long periods of low velocity and short episodes of high velocities. This intermittent behavior can be traced back to the fact, that particle velocities vary on a characteristic spatial scale rather than a temporal scale. Thus, intermittency can be removed by equidistant instead of isochronous velocity sampling. *Shapiro and Cvetkovic* [1988] considered the statistics of Lagrangian velocities sampled equidistantly along the mean flow direction. Later, *Le Borgne et al.* [2007] analyzed the evolution of equidistant Lagrangian velocity statistics to characterize the flow field organization. *Gotovac et al.* [2009] used equidistant statistics to characterize flow and travel time statistics. *Cvetkovic et al.* [1991] analyzed isochronous and equidistant Lagrangian velocities in one-dimensional steady flow.

Here, we consider velocity series as a function of the streamwise distance. The distance $s(t, \mathbf{a})$ traveled by a particle along a streamline is given by [*Dentz et al.*, 2016]

$$\frac{ds(t, \mathbf{a})}{dt} = v_t(t, \mathbf{a}). \quad (7)$$

where $v_t(t, \mathbf{a}) = |\mathbf{v}(t, \mathbf{a})|$ is the magnitude of the Lagrangian velocity. Applying the variable transform $t \rightarrow s$ based on (7), the equation of motion (6) transforms into the system of equations

$$\frac{d\mathbf{x}(s, \mathbf{a})}{ds} = \frac{\mathbf{v}_s(s, \mathbf{a})}{v_s(s, \mathbf{a})}, \quad \frac{dt(s, \mathbf{a})}{ds} = \frac{1}{v_s(s, \mathbf{a})}. \quad (8)$$

where $\mathbf{v}_s(s, \mathbf{a}) = \mathbf{q}[\mathbf{x}(s, \mathbf{a})]$ is termed the s(pace)-Lagrangian velocity because it varies with distance along the streamline. Its magnitude is denoted by $v_s(s, \mathbf{a}) = |\mathbf{v}(s, \mathbf{a})|$. The particle travel time at the distance s along the streamline is denoted by $t(s, \mathbf{a})$. The particle velocity $v_t(t, \mathbf{a})$ is given in terms of $v_s(s, \mathbf{a})$ as $v_t(t, \mathbf{a}) = v_s[s(t, \mathbf{a}), \mathbf{a}]$. Note that the transformation $t \rightarrow s$ converts the streamline length s into an independent variable just like time t in Eq. (6). Time t on the other hand, is converted into the dependent Lagrangian variable $t(s, \mathbf{a})$.

Figure 1 compares velocity series as a function of travel time and travel distance along a streamline for particle motion in heterogeneous porous medium. The intermittent behavior observed for $v_t(t, \mathbf{a})$ is removed for $v_s(s, \mathbf{a})$, which shows a regular random pattern. Thus, instead of the more complex t-Lagrangian velocity series, we focus in Section 4 on the modeling of the relatively simpler regular random pattern of $v_s(s, \mathbf{a})$ as a Markov process. Note that the mechanisms causing intermittency are the same for 2- and 3-dimensional porous media.

2.2.1 Lagrangian velocity distributions

We focus on the statistics of the magnitudes $v_t(t, \mathbf{a})$ and $v_s(s, \mathbf{a})$ of the t- and s-Lagrangian velocities. The following definitions and relations are valid for flow and particle velocities in 2- and 3-dimensional porous media. The t-Lagrangian velocity PDF is defined by isochronous sampling along a streamline as

$$p_t(v, \mathbf{a}) = \lim_{T \rightarrow \infty} \frac{1}{T} \int_0^T dt \delta[v - v_t(t, \mathbf{a})]. \quad (9)$$

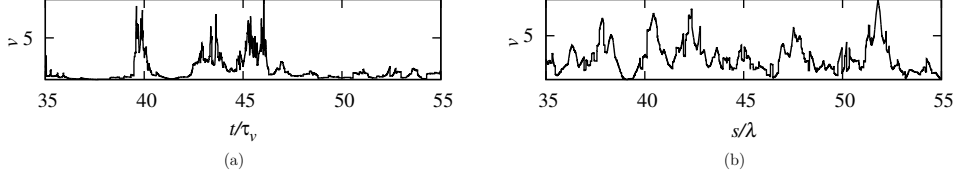


Figure 1: Lagrangian velocity time and space series along a particle trajectory for Darcy flow field in a Gamma K field with $\alpha = 0.5$.

Assuming Lagrangian ergodicity, the PDF is independent of the initial position and equal to the PDF obtained by sampling particle velocities from an ensemble of particles defined by their initial positions \mathbf{a} ,

$$p_t(v) = \lim_{V_0 \rightarrow \infty} \frac{1}{V_0} \int_{\Omega_0} d\mathbf{a} \delta[v - v_t(t, \mathbf{a})] \quad (10)$$

where Ω_0 is the injection domain and V_0 its volume. Note that the distribution of initial particle positions is uniform. The s-Lagrangian PDF is defined accordingly by equidistant sampling along a streamline as

$$p_s(v, \mathbf{a}) = \lim_{L \rightarrow \infty} \frac{1}{L} \int_0^L ds \delta[v - v_s(s, \mathbf{a})]. \quad (11)$$

Assuming ergodicity, the s-Lagrangian velocity distribution is independent of the initial position and equals the ensemble s-Lagrangian PDF

$$p_s(v) = \lim_{V_0 \rightarrow \infty} \frac{1}{V_0} \int_{\Omega_0} d\mathbf{a} \frac{v_0(\mathbf{a})}{\langle v_e \rangle} \delta[v - v_s(s, \mathbf{a})], \quad (12)$$

where $v_0(\mathbf{a}) = v_s(s=0, \mathbf{a}) = v_t(t=0, \mathbf{a})$ is the initial particle velocity. Note that here the initial particle distribution is flux-weighted, this means

$$\rho(\mathbf{a}) = \frac{1}{V_0} \frac{v_0(\mathbf{a})}{\langle v_e \rangle}. \quad (13)$$

2.2.2 Relationships between Eulerian and Lagrangian velocity distributions

Volume conservation implies that the ensemble t-Lagrangian velocity PDF (10) and Eulerian velocity PDF (5) are equal. This can be seen by using the variable transformation $\mathbf{a} \rightarrow \mathbf{x}(t, \mathbf{a})$ in (10) and noting that volume conservation implies that the Jacobian of the transformation is unity,

$$p_t(v) = \lim_{V_0 \rightarrow \infty} \frac{1}{V_0} \int_{\Omega(t)} d\mathbf{x} \delta[v - v_e(\mathbf{x})] = p_e(v). \quad (14)$$

The relation between the s-Lagrangian and t-Lagrangian PDFs can be obtained by the variable transform $s \rightarrow t(s)$ in (12), which gives

$$p_s(v) = \lim_{L \rightarrow \infty} \frac{T(L)}{L} \frac{1}{T(L)} \int_0^{T(L)} dt v \delta[v - v_t(t, \mathbf{a})] = \frac{v}{\langle v_e \rangle} p_t(v). \quad (15)$$

Field	λ [m]	L_x	L_y	$\Delta x, \Delta y$	μ_f	σ_f^2	α	k_0 [m/s]	k_c [m/s]
Lognormal	10	600λ	150λ	$\lambda/10$	0	0.1–7	-	-	-
Gamma		300λ	300λ		-2.95 – -4.57	1.9–11.7	0.3–0.9	10^{-11}	5

Table 1: Summary of the numerical setup, the discretization of the multi-Gaussian K fields and parameter values for the Lognormal and Gamma fields considered in this study.

The s-Lagrangian and t-Lagrangian PDFs are related through flux-weighting. This can be understood as follows. Isochrone sampling gives more weight on slow velocities than on high velocities, while equidistant sampling gives the same weight to all velocities as illustrated in Figure 1.

Relation (15) implies together with (14) that the s-Lagrangian PDF is related to the Eulerian PDF through flux-weighting as [Dentz *et al.*, 2016]

$$p_s(v) = \frac{v}{\langle v_e \rangle} p_e(v). \quad (16)$$

This is a key relationship because it relates the s-Lagrangian PDF, a transport attribute, to the Eulerian PDF, a flow attribute, which can be measured independently of transport. Equation (16) may be illustrated as follows. As low velocities occupy wider streamtubes than high velocities, spatial sampling results in higher frequencies of low velocities. Equidistant sampling along trajectory, however, gives equal weight to low and high velocities. Note that this key result and its derivation are valid for 2- and 3-dimensional porous media. Note that relations (14)-(16) hold under stationary conditions. This means, the stationary t-Lagrangian distribution is equal to the Eulerian PDF and the stationary s-Lagrangian distribution is equal to the flux-weighted Eulerian PDF.

2.3 Numerical simulations

Stochastic simulations are based on the Monte-Carlo method. The groundwater flow equation is solved for multiple realizations of $K(\mathbf{x})$, which belong to an ensemble characterized by the same statistical properties. Transport is solved by particle tracking. Flow and transport statistics and average behaviors are obtained by spatial sampling and streamwise sampling in individual realization and by sampling between medium realizations. We describe in the following the direct numerical simulations (DNS) of Darcy flow and transport in heterogeneous porous media. We explain the methods used to generate hydraulic conductivity fields $K(\mathbf{x})$ as spatial stochastic processes based on multi-Gaussian random field $Y(\mathbf{x})$, the hydraulic setting used for the flow simulations and the particle tracking method used to simulate transport.

2.3.1 Field generation

Isotropic multi-Gaussian random fields $Y(\mathbf{x})$ characterized by zero mean and the exponential covariance function (3) are generated on a regular grid in two dimensions using the Random Fields Package [Schlather *et al.*, 2015] of the R software environment [R Core Team, 2015]. Table 1 summarizes field dimensions, discretization and point distribution details for K . We consider Lognormal and truncated Gamma distributions for the marginal distribution $p_K(k)$ of $K(\mathbf{x})$. The Lognormally distributed $K(\mathbf{x})$ is obtained from $Y(\mathbf{x})$ from the pointwise map $K(\mathbf{x}) = \exp[Y(\mathbf{x})]$. The truncated Gamma distributed $K(\mathbf{x})$ is obtained by inverse transform sampling or Smirnov transform as

$$K(\mathbf{x}) = P_K^{-1}(\Phi[Y(\mathbf{x})]), \quad (17)$$

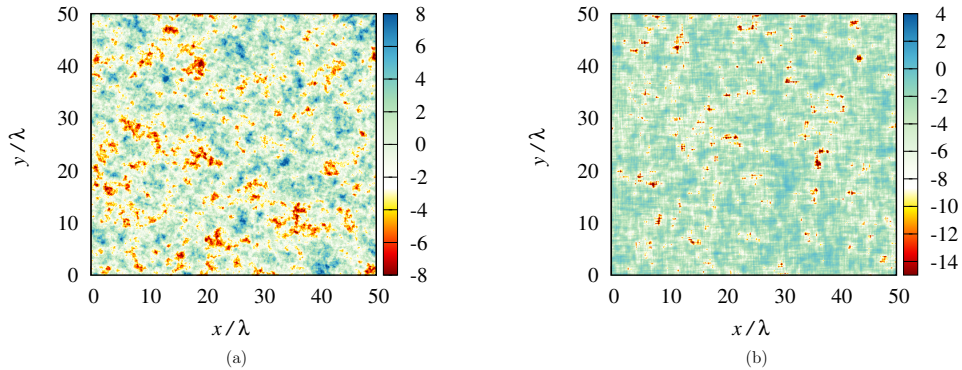


Figure 2: Realizations of the two types of K fields considered in this study. For the Lognormal field $\sigma_Y^2 = 7$ and for the Gamma field $\alpha = 0.5$.

where $\Phi(y)$ is the cumulative distribution function (CDF) of the Gaussian distribution and $P_K^{-1}(u)$ is the inverse CDF of the truncated Gamma distribution. This robust method can be used when the inverse CDF lacks a closed-form analytical solution, which is the case for the truncated Gamma distribution (4). In short, this is a two step method: 1) the random variable $Y(\mathbf{x})$ is mapped onto a uniformly distributed random variable using the CDF $\Phi(y)$, and 2), the uniform random variable is mapped onto the target variable $K(\mathbf{x})$ through inverse sampling. The inverse transform sampling is implemented in an in-house C++ code based on the binary search algorithm from the GNU Scientific Library [Galassi *et al.*, 2016]. The Monte-Carlo simulations use 100 realizations of each random field.

Figure 2 illustrates the typical structure of the hydraulic conductivity field for the Lognormal and truncated Gamma-distributed K fields. For both fields, the correlation structure is exponential, which induces a sharp contrast for neighboring K values. The heterogeneous distributions show different spatial organization. The Lognormal based field presents typical areas of high and low K values. The structure of the Gamma based K field is similar, but is characterized by sparse regions of extremely low K values.

2.3.2 Groundwater flow

Direct numerical simulations (DNS) of saturated Darcy flow are performed in steady-state with a reference permeameter-like setting [Bellin *et al.*, 1992; de Dreuzy *et al.*, 2007b; Gotovac *et al.*, 2009]. Fixed pressure boundary conditions are applied to the upstream (left) and downstream (right) boundaries with a unit head drop; no-flow conditions are applied to the top and bottom boundaries. The groundwater flow equation

$$\nabla^2 h(\mathbf{x}) + \nabla \cdot [Y(\mathbf{x})\nabla h(\mathbf{x})] = 0 \quad (18)$$

based on finite volume [Eftekhari, 2015] with a discretization of $\lambda/10$. The inter-cell hydraulic conductivity is set equal to the harmonic mean. To ensure stationarity of the Eulerian velocity statistics, we consider an inner sub-domain which is limited by a biased belt of width 25λ . Such a width is sufficient for the most heterogeneous fields with $\sigma_Y^2 \leq 7$ as discussed in Appendix A: . Flow is uniform in the mean and directed along the x_1 -direction of the coordinate system. We verified the accuracy of the flow simulations by comparing the variance of the Eulerian velocity component along the mean flow direction to reference simulations [de Dreuzy *et al.*, 2007b; Gotovac *et al.*, 2009]. The statistics of our simulations (variance along the mean flow direction) agree very well with these references, see Appendix A: .

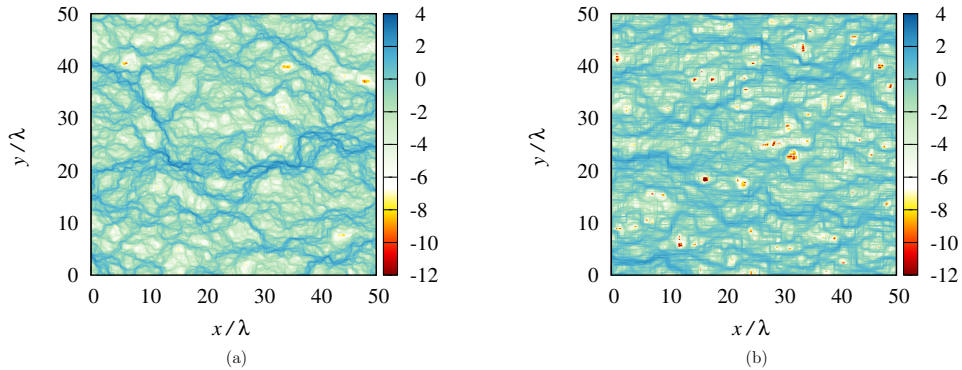


Figure 3: Map of the natural logarithm of the velocity magnitude corresponding to the conductivity fields in Figure 2.

2.3.3 Particle tracking

Unlike classical particle tracking methods, which solve the equations of motion (6) by discretization in time, our method is based on the equation of motion (8), which describes particle motion as a function of travel distance s along a streamline. The particle trajectory $\mathbf{x}(s, \mathbf{a})$ is obtained numerically from

$$\mathbf{x}_{n+1} = \frac{\mathbf{q}[\mathbf{x}_n]\Delta s}{|\mathbf{q}(\mathbf{x}_n)|}, \quad t_{n+1} = t_n + \frac{\Delta s}{|\mathbf{q}[\mathbf{x}_n]|}, \quad (19)$$

where we set $\mathbf{x}_n = \mathbf{x}(n\Delta s, \mathbf{a})$ and $t_n = t(n\Delta s, \mathbf{a})$. This method can be considered a time-domain random walk [Noetinger *et al.*, 2016]. It is of advantage in scenarios, which are characterized by the presence of regions of very low velocities as it the case in this study because the number of steps does not depend on the local velocity value as in time-stepping methods. We choose the discretization $\Delta s = \lambda/10^3$. The series of s-Lagrangian velocities is given by $v_s(n\Delta s, \mathbf{a}) = |\mathbf{q}(\mathbf{x}_n)|$. The series of t-Lagrangian velocities is given by

$$v_t(t, \mathbf{a}) = v_s(n_t\Delta s, \mathbf{a}), \quad (20)$$

where $n_t = \max(n | t_n \leq t)$. Flow velocities within the finite volume cells are obtained using a bilinear interpolation of the velocities at cell faces [Pollock, 1988]:

$$q_x(\mathbf{x}) = A_x(x - x_L) + q_x(x_L) \quad (21)$$

$$q_y(\mathbf{x}) = A_y(y - y_B) + q_y(y_B), \quad (22)$$

where

$$A_x = [q_x(x_R) - q_x(x_L)]/d_x \quad (23)$$

$$A_y = [q_y(y_T) - q_y(y_B)]/d_y \quad (24)$$

where x_L , x_R , y_B and y_T are the positions of the left, right, bottom and top boundaries of the cell, respectively and d_x and d_y are the cell sizes, which here are equal, $d_x = d_y = \lambda/10$.

3 Lagrangian velocity statistics

In this section we study the evolution of the Lagrangian velocity statistics both in terms of travel time and travel distance along streamlines and their relation to the Eulerian velocity statistics discussed in Section 2.2.2. In Section 2.2.1, we have defined the

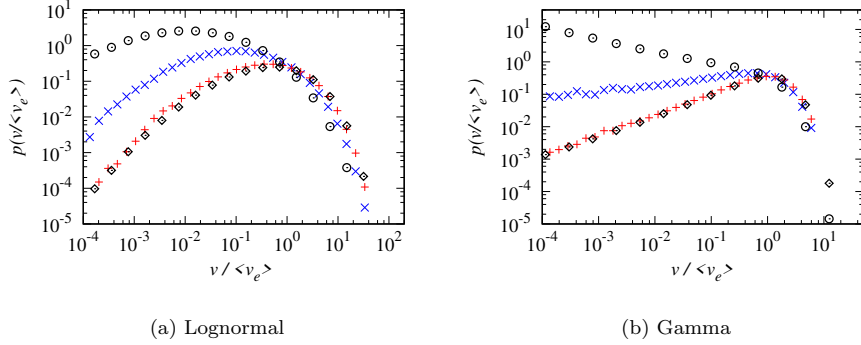


Figure 4: Evolution of the space-Lagrangian velocity PDF from the Eulerian initial velocity PDF (top, black circles) to the flux-weighted Eulerian velocity PDF (bottom, black diamonds). The intermediate s-Lagrangian velocity PDFs are sampled at distances of $s = 2\lambda$ (blue crosses) and $s = 10\lambda$ (red crosses).

ensemble t- and s-Lagrangian PDFs (10) and (12) for uniform and flux-weighted injection conditions, respectively. Under ergodic injection conditions, these initial conditions correspond to the stationary distributions of the t- and s-Lagrangian statistics. We mean by ergodic injection conditions that the injection domain is large enough such that the initial velocity PDF is equal to the Eulerian velocity PDF,

$$\frac{1}{V_0} \int_{\Omega_0} d\mathbf{a} \delta[v - v_0(\mathbf{a})] = p_e(v), \quad (25)$$

which for the stationary flow fields under consideration here is fulfilled by definition for $V_0 \rightarrow \infty$. We consider injections over line extensions $\geq 10^2\lambda$.

Here, we will investigate the evolution of Lagrangian velocity statistics. Thus, we define the transient t- and s-Lagrangian PDFs as

$$\hat{p}_t(v, t) = \int d\mathbf{a} \rho(\mathbf{a}) \delta[v - v_t(t, \mathbf{a})] \quad (26)$$

$$\hat{p}_s(v, s) = \int d\mathbf{a} \rho(\mathbf{a}) \delta[v - v_s(s, \mathbf{a})], \quad (27)$$

where $\rho(\mathbf{a})$ is the distribution of initial particle positions. The initial velocity distribution is denoted by $p_0(v) = p_t(v, t = 0) = p_s(v, s = 0)$. It is related to the initial particle distribution $\rho(\mathbf{a})$ as

$$p_0(v) = \int d\mathbf{a} \rho(\mathbf{a}) \delta[v - v_0(\mathbf{a})]. \quad (28)$$

Within a Lagrangian stochastic framework, the knowledge of the Lagrangian velocity statistics is crucial for transport predictions, see Eq. (6)-(8). For the determination of the solute breakthrough curves, for example, it is more convenient to consider the slowness $w = 1/v_s$ [Gotovac *et al.*, 2009]. The statistics of $w = 1/v_s$ can be obtained from the statistics of v_s by variable transform. The PDF $\hat{p}_w(w, s)$ of $w(s)$ is given in terms of $\hat{p}_s(v, s)$ by

$$\hat{p}_w(w, s) = \frac{1}{w^2} \hat{p}_s(1/w, s). \quad (29)$$

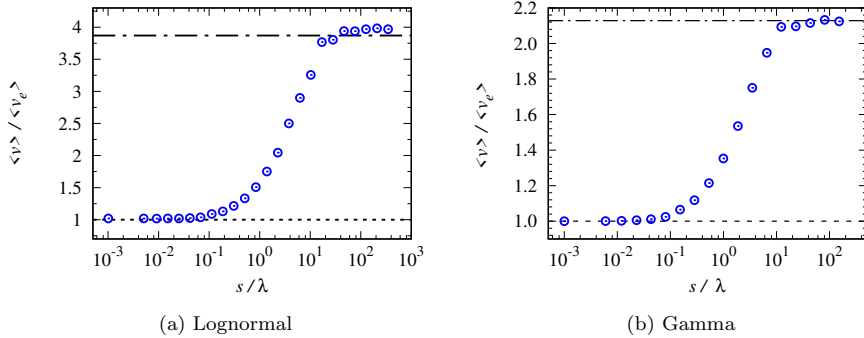


Figure 5: Evolution of the space-Lagrangian velocity mean for a uniform initial particle distribution. The mean increases from the mean of the Eulerian velocity (lower dotted line) to the mean of the flux-weighted Eulerian velocity (upper dashed dotted line).

Specifically, at steady state, we obtain through the flux-weighting relation (16) between $p_s(v)$ and $p_e(v)$ for the steady state PDF $p_w(w)$ of slowness

$$p_w(w) = \frac{1}{w^3 \langle v_e \rangle} p_e(1/w). \quad (30)$$

Hence, the slowness statistics is also fully determined by Eulerian statistics, this means by a flow attribute.

In the following, we investigate the evolution of t- and s-Lagrangian velocities for Lognormal and truncated-Gamma distributed hydraulic conductivity fields. For illustration, we show the behaviors for two heterogeneous cases: $\sigma_Y^2 = 7$ for the Lognormal field and $\alpha = 1/2$ for the Gamma field. The behaviors for other parameter values are qualitatively similar.

3.1 Evolution of s-Lagrangian velocities

As pointed out above, the space-Lagrangian velocity PDF evolves if solute particles are injected with a distribution different from its steady-state, the flux weighted Eulerian velocity PDF (16). Figure 4 shows the evolution of the s-Lagrangian velocity PDF for a uniform injection of particles in the two types of K fields under consideration. For this injection mode, the main features of the evolution of the probabilities are a decrease for low velocities and an increase for high velocities. These opposite evolutions reflect the convergence towards the flux-weighted Eulerian velocity PDF in which high velocities are dominating. A cautious comparison of the two figures reveals a difference. For the larger travel distance, $s = 10\lambda$, the velocity PDF does not completely coincide with the steady-state velocity PDF for the Lognormal K field, while this overlap exists for the Gamma field. This difference reflects that the correlation length of s-Lagrangian velocities is greater in the Lognormal-field than in the Gamma-field. Since both fields have a similar variance, this difference in correlation length relates to the heterogeneity in the distribution of the hydraulic conductivity. We shall discuss this point further in Section 5. Now, we focus our analysis on the evolution of the mean s-Lagrangian velocity,

$$\langle v_s(s) \rangle = \int_0^\infty dv v \hat{p}_s(v, s). \quad (31)$$

Figure 5 shows the evolution of the mean s-Lagrangian velocity for a uniform injection. According to this injection mode, the mean of the initial s-Lagrangian velocity

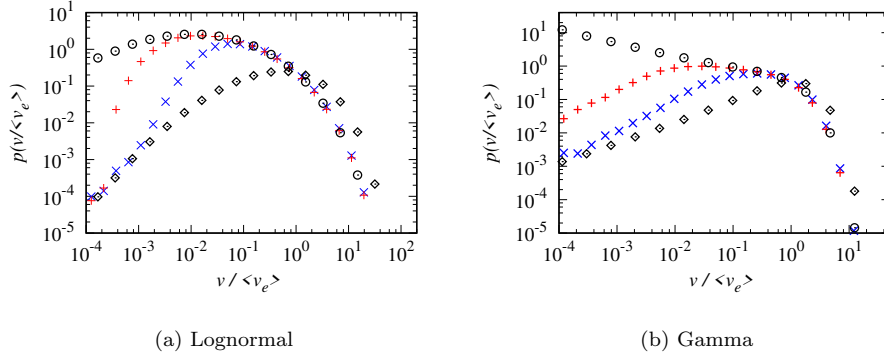


Figure 6: Evolution of the time-Lagrangian velocity PDF. The PDF evolves from the flux-weighted Eulerian velocity PDF (bottom black diamonds) to the Eulerian velocity PDF (top black circles). For the Lognormal-field, the two intermediate velocity PDFs are at $t = 20\tau_u$ (blue crosses) and $t = 200\tau_u$ (red crosses); for the Gamma field, intermediate times are: $t = 5.5\tau_u$ (blue crosses) and $t = 33\tau_u$ (red crosses).

PDF is the arithmetic mean of the Eulerian velocity PDF. Similar to the evolution of the PDF, the mean of the s-Lagrangian velocity evolves between the Eulerian and flux-weighted Eulerian mean at short and long distances respectively. When the injection distribution differs from the steady-state distribution, the mean of the s-Lagrangian velocity PDF is determined by the initial velocity distribution and converges toward the mean of the steady-state s-Lagrangian velocity PDF.

3.2 Evolution of t-Lagrangian velocities

In Section 2.2.2 we saw that the steady-state t-Lagrangian velocity PDF is equal to the Eulerian velocity PDF, see Eq. 14. Thus, if the initial t-Lagrangian velocity PDF differs from the uniform injection, the t-Lagrangian velocity PDF shall converge to the steady-state velocity PDF with time.

Figure 6 shows the temporal evolution of the t-Lagrangian velocity PDF to its steady-state. The PDF evolves from an initial flux-weighted velocity PDF to the steady-state Eulerian velocity PDF. According to this injection mode, particles are injected proportional to the local flow. The initial ($t = 0$) velocity distributions have low and high probabilities for the low and high velocities respectively. At intermediate times, probabilities of low velocities persist close to their initial values. For high velocities, $\hat{p}_t(v, t)$ is close to the steady-state velocity PDF. This difference suggests that probabilities of high velocities reach steady-state faster than the probabilities of low velocities. Indeed, particles persist long times at low velocities which give rise to strong correlation. As mentioned in the Introduction and in Section 2.2, long persistence times result in memory effects and intermittency, see also Figure 1. At the later time, the convergence of probabilities for very low velocities remains incomplete. This intermittent feature is complex to model in time because it requires the characterization of the memory effects. Conversely, the space sampled velocities show no intermittency and require lower levels of characterization. This is why we consider in the following the spatial framework.

4 Markov models for the evolution of Lagrangian velocities

As seen in Section 2.2 and the previous section, the s-Lagrangian velocity series fluctuates on a characteristic length scale ℓ_c , and the s-Lagrangian velocity statistics evolve

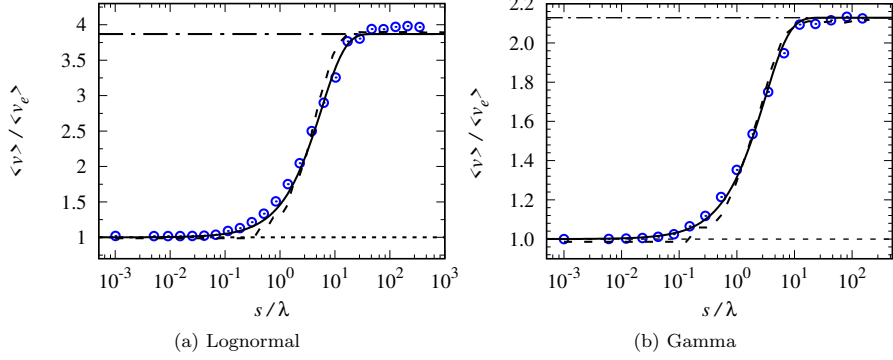


Figure 7: Evolution of the space-Lagrangian velocity mean for a uniform initial particle distribution. The mean increases from the mean of the Eulerian velocity (lower dotted line) to the mean of the flux-weighted Eulerian velocity (upper dashed dotted line). The solid line denotes the Bernoulli model for (Lognormal) $\ell_c = 5.7\lambda$ and (Gamma) $\ell_c = 3.1\lambda$. The dashed line denotes the Ornstein-Uhlenbeck model for (Lognormal) $\ell_c = 3.5\lambda$ and (Gamma) $\ell_c = 2.1\lambda$.

towards stationarity within a few ℓ_c . Due to the relative simplicity of the s-Lagrangian velocity series compared to the intermittent t-Lagrangian velocities, here we focus on the modeling of $v_s(s, \mathbf{a})$ as stationary Markov processes. This means, the velocity series $v_s(s, \mathbf{a})$ of single particle is represented as a realization of a stochastic processes $\{v_s(s)\}$. In this framework, the particle time is evolving along the streamline as

$$\frac{dt(s)}{ds} = \frac{1}{v_s(s)}. \quad (32)$$

The t-Lagrangian velocity is given by $v_t(t) = v_s[s(t)]$ with $s(t) = \max[s|t(s) \leq t]$. The evolution of $\hat{p}(v, s)$ is described by the Chapman-Kolmogorov equation

$$\hat{p}_s(v, s + \Delta s) = \int_0^\infty dv' r(v, \Delta s|v') \hat{p}_s(v', s), \quad (33)$$

where $r(v, \Delta s|v')$ is the transition probability density, which characterizes the Markov process. The t-Lagrangian PDF $\hat{p}_t(v, t)$ can be expressed in terms of the s-Lagrangian statistics as [Dentz *et al.*, 2016]

$$\hat{p}_t(v, t) = v^{-1} \int_0^\infty ds R(v, t, s), \quad (34)$$

where $R(v, t, s)$ is the joint PDF of finding a particle with velocity v and time t after a streamwise distance s . The initial velocity distribution $\hat{p}_s(v, s = 0) = p_0(v)$ is given by (28). Note that in this framework, the injection mode is accounted for by the initial particle velocity.

In the following, we quantify the evolution of the s-Lagrangian velocity by two stochastic relaxation models, a Bernoulli velocity model and an Ornstein-Uhlenbeck model. These models are compared to the direct numerical simulations (DNS) of flow and transport in the Lognormal and Gamma-distributed hydraulic conductivity fields. For illustration, we show the comparisons for the Lognormal model with $\sigma_Y^2 = 7$ and the Gamma model with $\alpha = 1/2$.

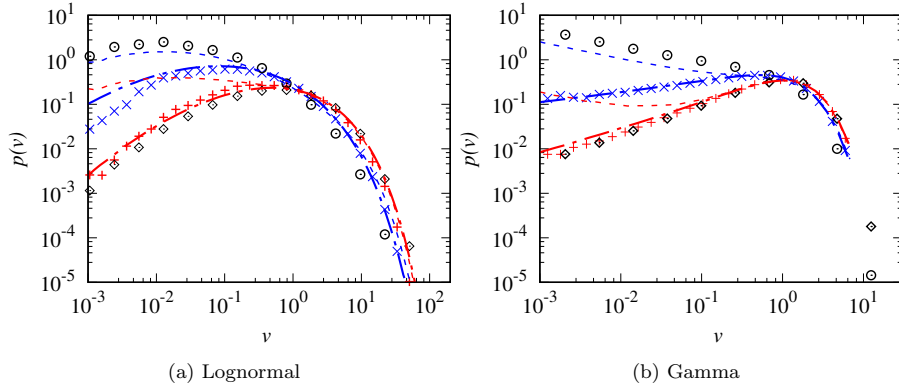


Figure 8: Evolution of the velocity PDF from (symbols) the DNS and (dashed lines) prediction by (dashed) expression (36) for the Bernoulli model, and (dashed-dotted) the Ornstein-Uhlenbeck model. The correlation lengths ℓ_c are the same as in Figure 7.

4.1 Bernoulli model

To quantify the evolution of the space-Lagrangian velocity distribution we follow the approach based on the Bernoulli velocity model [Dentz *et al.*, 2016]

$$v_{n+1} = v_n \xi_n + \eta_n (1 - \xi_n), \quad (35)$$

where $v_n = v_s(n\Delta s)$. ξ_n is a Bernoulli process which takes the values $\xi_n = 1$ with probability $\exp(-\Delta s/\ell_c)$ and 0 else. ℓ_c is the correlation length of velocities along the trajectory and the velocity η_n is distributed according to the steady state PDF $p_s(v)$. Thus, the evolution of $\hat{p}_s(v, s)$ is given by the exponential relaxation model

$$\hat{p}_s(v, s) = p_s(v) + \exp(-s/\ell_c) [p_0(v) - p_s(v)]. \quad (36)$$

The decay from the initial Lagrangian velocity distribution $p_0(v)$ to the steady-state distribution $p_s(v)$ is exponential. The decay rate ℓ_c^{-1} is constant and thus velocity independent. This independence sheds light on the nature of the evolution of s-Lagrangian velocity PDF, which shall be discussed below.

The evolution of the mean velocity is obtained from Equation (36) as

$$\langle v_s(s) \rangle = \langle v_s \rangle + \exp(-s/\ell_c) [\langle v_0 \rangle - \langle v_s \rangle]. \quad (37)$$

Figure 7 shows a comparison of the mean s-Lagrangian velocity obtained by the DNS and expression (37), where we fitted the correlation length ℓ_c , the only free parameter in this model. However, ℓ_c is related to the correlation length λ of $Y(\mathbf{x})$ and the heterogeneity strength as discussed below. For both types of K fields, the Bernoulli model reproduces the evolution obtained by DNS. This relaxation model quantifies the evolution of the mean of the s-Lagrangian velocity PDFs. Since the mean velocity represents merely the central tendency of the velocity distribution, it remains to be verified if the Bernoulli model predicts the evolution of the entire PDF.

Figure 8 shows the evolution of $\hat{p}(v, s)$ given by the DNS and expression (36). The evolution from the initial PDF $p_0(v)$ to the steady state $p_s(v)$ is captured by definition of the model. At intermediate distances, (36) represents well the convergence rate at high velocities, while it is too slow at low velocities. This result sheds light on the nature of the relaxation process. Since in the Bernoulli model the convergence rate is constant, the difference between model and DNS suggests that the convergence rate of the s-Lagrangian

velocity PDF is velocity dependent. The Bernoulli model is not able to predict the evolution of the s-Lagrangian velocity PDF at intermediate distances.

4.2 Ornstein-Uhlenbeck model

We consider now a more complex model to account for the velocity dependence in the evolution of s-Lagrangian velocity PDF. Specifically, we consider the evolution of $v_s(s)$ based on an Ornstein-Uhlenbeck process [Massouديه *et al.*, 2017; Morales *et al.*, 2017]. The s-Lagrangian velocity here is obtained according to the bijective map

$$v(s) = F[w(s)] \quad (38)$$

from the Gaussian process $w(s)$. Note that $w(s)$ is the normal score of $v(s)$. The process $w(s)$ satisfies the Langevin equation [Gardiner, 1985]

$$\frac{dw(s)}{ds} = -\ell_c^{-1}w(s) + \sqrt{2\ell_c}\xi(s), \quad (39)$$

where $\xi(s)$ is a Gaussian white noise with zero mean and covariance $\langle \xi(s)\xi(s') \rangle = \delta(s-s')$. Thus, $w(s)$ is modeled here as an Ornstein-Uhlenbeck process. The distribution $\hat{p}_w(w, s)$ of $w(s)$ evolves according to the Smoluchowski equation

$$\frac{\partial \hat{p}_w(w, s)}{\partial s} = \frac{\partial}{\partial w} \ell_c^{-1}w \hat{p}_w(w, s) + \ell_c \frac{\partial^2}{\partial w^2} \hat{p}_w(w, s). \quad (40)$$

Its steady state distribution $p_w(w)$ is given by the Gaussian

$$p_w(w) = \frac{\exp\left(-\frac{w^2}{2}\right)}{\sqrt{2\pi}}. \quad (41)$$

Thus, the map $F(w)$ reads as

$$F(w) = P_s^{-1}[\Phi(w)], \quad (42)$$

where $\Phi(w)$ is the cumulative distribution function (CDF) of the Gaussian distribution and $P_s^{-1}(u)$ is the inverse CDF of the steady state velocity distribution $P_s(v)$. This map guarantees that the velocity statistics converges to its steady state $p_s(v)$.

The evolution of $w_n = w(n\Delta s)$ in discrete steps Δs is given by the discretized version of (39),

$$w_{n+1} = w_n(1 - \ell_c^{-1}\Delta s) + \sqrt{2\ell_c\Delta s}\xi_n, \quad (43)$$

where the ξ_n are independent identically distributed Gaussian random variables characterized by 0 mean and unit variance. The initial values are given by $w_0 = F^{-1}(v_0)$, where the initial velocities are distributed according to $p_0(v)$. The evolution of v_n thus is given by

$$v_{n+1} = F \left[F^{-1}(v_n)(1 - \ell_c^{-1}\Delta s) + \sqrt{2\ell_c\Delta s}\xi_n \right]. \quad (44)$$

As in the Bernoulli model, the only free parameter here is the correlation distance ℓ_c , which, however, is related to the correlation length and heterogeneity strength of the underlying random field $Y(\mathbf{x})$ as discussed below. As here we do not have a closed form analytical solution for the mean velocity $\langle v_s(s) \rangle$, the correlation length is estimated from the evolution of $\langle w(s) \rangle$ as outlined in Appendix B: .

Figure 7 shows the evolution of the mean velocity $\langle v_s(s) \rangle$ based on the Ornstein-Uhlenbeck process. The model provides a good description of the evolution of the mean velocity from its initial to steady state values. Figure 8 shows the evolution of s-Lagrangian

velocity PDF predicted by the Ornstein-Uhlenbeck model. It addresses the issue of the Bernoulli model, which is not able to reproduce the evolution at low velocities. The simulated velocity PDF now agrees with the PDF obtained by DNS for both high and low velocities. Note that the convergence rate ℓ_c^{-1} as well as the noise term in the Ornstein-Uhlenbeck model (39) are state-independent. This is not the case for the evolution of $v_s(s)$ described by (44). Both convergence rate and noise strength for the latter are in general velocity dependent. This can be seen by Taylor expanding the right side of (44) up to linear order in Δs , which gives

$$v_{n+1} = v_n - A(v_n)\ell_c^{-1}\Delta s + B(v_n)\ell_c\Delta s + C(v_n)\sqrt{2\ell_c\Delta s}\xi_n, \quad (45)$$

where we implicitly use the Ito interpretation of the stochastic integral [*Gardiner*, 1985], and defined

$$A(v) = \frac{dF[F^{-1}(v)]}{dw}F^{-1}(v), \quad B(v) = \frac{d^2F[F^{-1}(v)]}{dw^2}, \quad C(v) = \frac{dF[F^{-1}(v)]}{dw}. \quad (46)$$

4.3 Synthesis

We have modeled the s-Lagrangian velocities as a Markov process, which is fully determined by the Eulerian velocity PDF, a flow attribute independent from transport, and the correlation length, which depends on the medium properties. The Markov approach is predictive in the sense that it relates flow and medium properties with large scale transport in terms of stochastic evolution equations for the s-Lagrangian velocities. Velocity transitions and thus the evolution of the the velocity statistics depend on the specific Markov model under consideration. We have considered two Markov models of different complexity, a Bernoulli process for the velocity transitions and an Ornstein-Uhlenbeck process for the transitions of the normal scores of velocity. While both models capture the evolution of the s-Lagrangian velocity statistics qualitatively, the Bernoulli process does not predict accurately the preasymptotic velocity PDFs at small velocities. The Ornstein-Uhlenbeck process in contrast provides an accurate quantitative prediction of the evolution of $\hat{p}(v, s)$. Nevertheless, the Bernoulli process is appealing due to its simplicity and analytical tractability [*Dentz et al.*, 2016], which allows to obtain a closed form expression for large scale dispersion. As it provides an accurate prediction of the evolution of intermediate and high velocities and the asymptotic statistics, it may provide a robust model for certain transport aspects.

5 Hydraulic conductivity distribution and velocity statistics

In this section, we focus on the dependence of the correlation length ℓ_c on the variance σ_f^2 of the logarithm of K and the relation to λ , the correlation length of the underlying multi-Gaussian $Y(\mathbf{x})$ in both the Lognormal and Gamma fields, and the comparison of the pointwise K PDF and the pointwise PDF of the Eulerian velocity magnitude.

5.1 Correlation length of s-Lagrangian velocities

We determine the correlation length ℓ_c estimated from the Bernoulli process from expression (37) and from the Ornstein-Uhlenbeck model as outlined in Appendix B: as a function of the heterogeneity of the K field measured in terms of the variance σ_f^2 of the logarithm of K . Figure 9 reveals that for both the Lognormal and Gamma fields ℓ_c is larger than the correlation length λ of $Y(\mathbf{x})$, and increases with increasing variance σ_f^2 . This is due to the fact that the tortuosity of the streamlines is larger than 1 and increases with increasing heterogeneity. Similar observations have been made by *Cvetkovic et al.* [1996] and *Le Borgne et al.* [2007]. The correlation length depends linearly on σ_f^2 . For the Lognormal fields, we find

$$\ell_c/\lambda = 0.181\sigma_f^2 + 2.221, \quad (47)$$

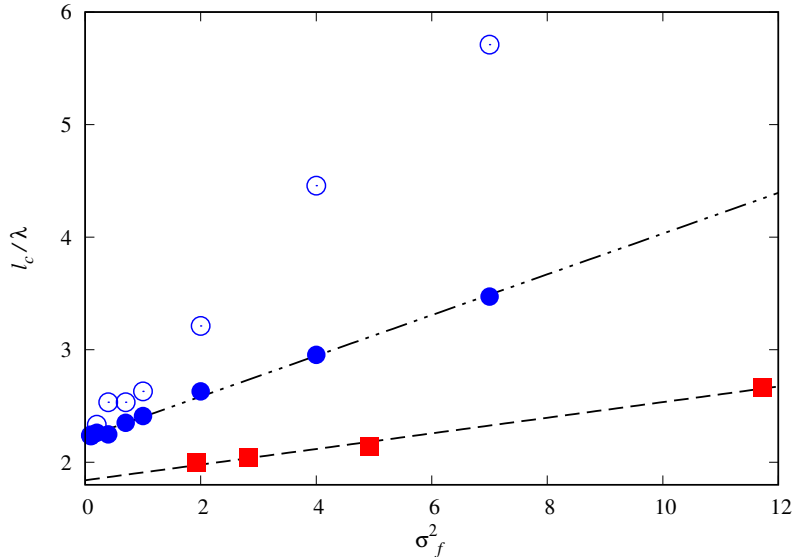


Figure 9: Correlation lengths for the (circles) Lognormal and (squares) Gamma fields estimated from the Ornstein-Uhlenbeck process and (open circles) correlation lengths for the Lognormal fields estimated from the Bernoulli model.

and for the Gamma fields,

$$\ell_c/\lambda = 0.069\sigma_f^2 + 1.840. \quad (48)$$

The correlation lengths for the Lognormal and Gamma fields are different for the same values of σ_f^2 , which indicates a dependence of ℓ_c on the conductivity point distribution because the correlation structure of the underlying multi-Gaussian field $Y(\mathbf{x})$ is the same. Changes of correlation structure, for instance high/low- K connected zones, is expected to impact transport on the Lagrangian flow attributes [Le Borgne et al., 2008b]. Figure 9 also shows the correlation lengths for the Lognormal fields estimated from the Bernoulli and Ornstein-Uhlenbeck models for the Lognormal fields. The correlation lengths for the Ornstein-Uhlenbeck model are smaller than for the Bernoulli model, which demonstrates the model dependence of ℓ_c .

5.2 Hydraulic conductivity and Eulerian velocity statistics

We discuss now the relationship between the PDFs of K and v_e . Several studies have found, or assume that the PDF of the magnitude of the flow velocity and the stream-wise flow components may be proportional to the PDF of hydraulic conductivity values [Bellin et al., 1992; Fiori et al., 2006, 2007; Cvetkovic et al., 2014; Ederly et al., 2014; Tyukhova et al., 2016] at least for values much smaller than the mean. The prediction of the low velocity end of $p_e(v)$ is valuable because low velocities induce long travel times and thus are at the origin of breakthrough curves tailing and anomalous transport in general. This observation can be explained by considering the flow in a single isolated inclusion [Eames and Bush, 1999; Fiori et al., 2006, 2007; Cvetkovic et al., 2014], which is given by

$$u_i = \frac{2u_m K_i}{K_m + K_i}, \quad (49)$$

where u_i is the velocity in the inclusion, u_m the velocity in the surrounding matrix and K_i and K_m correspondingly. For $K_i \ll K_m$, the velocity in the inclusion is $u_i \approx 2u_m K_i/K_m$

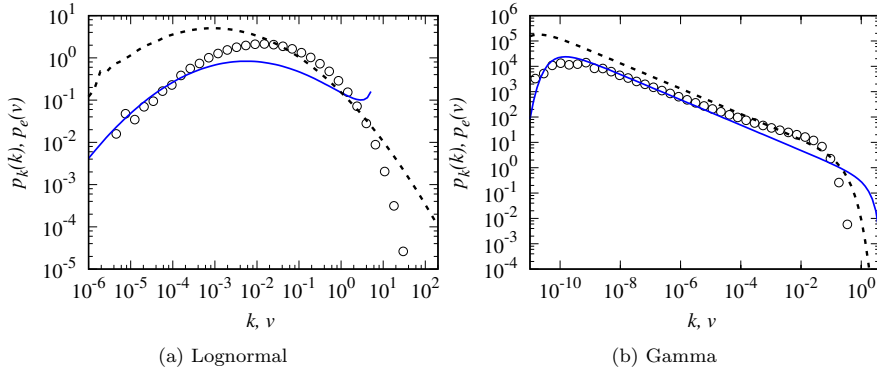


Figure 10: Comparison between (dashed lines) $p_K(k)$ for (a) Lognormal with $\sigma_f^2 = 7$ and (b) Gamma distribution with $\alpha = 0.5$, (symbols) $p_e(v)$ sampled from the DNS, (blue line) $p_e(v)$ given by (50) for the inclusion model with (a) $u_m = 3$ m/s and (b) $u_m = 3.75$ m/s.

and thus proportional to the hydraulic conductivity. *Fiori et al.* [2006, 2007] generalized this reasoning for media consisting of random distributions of inclusions of variable conductivity. Furthermore, one can argue that conductivity fields based on multi-Gaussian random fields have a similar structure as media consisting of inclusions because the topology of multi-Gaussian fields is characterized by islands of high and low values and connected regions with conductivities around the mean. Mapping of the conductivity PDF $p_K(k)$ onto $p_e(v)$ according to (49) gives

$$p_e(v) = \frac{2u_m}{(2u_m - v)^2} p_K[v/(2u_m - v)]. \quad (50)$$

Figure 10 shows a comparison between the conductivity distribution $p_K(k)$ of the Lognormal and Gamma distribution, the Eulerian velocity distribution $p_e(v)$ obtained from the DNS for the Lognormal and Gamma fields, and the corresponding expression (50) from the inclusion model. For the Lognormal field, we find that $p_e(v)$ and $p_K(k)$ actually compare relatively well over more than 2 orders of magnitude in the range of $K = 10^{-2} - 1$. The inclusion model performs relatively well for values $K < 10^{-3}$. For the Gamma field, the inclusion model performs relatively well for $K < 10^{-7}$ over several orders of magnitude. There is a certain correspondence between the conductivity PDF and PDF of the Eulerian velocity magnitude. While an exact map between $p_e(v)$ and $p_K(k)$ is still an open question, the inclusion model provides a good estimate for the behavior at small values of K while setting both PDFs simply equal provides relatively good estimates for intermediate K values around the mean for the Lognormal and Gamma fields.

6 Conclusions

We have conducted a thorough analysis of Lagrangian velocity statistics for steady flow through Darcy-scale heterogeneous porous media with the aim of identifying and quantifying the stochastic dynamics of particle velocities and thus large scale particle motion. In order to understand the stochastic velocity dynamics, we consider two statistics, which are defined in terms of the sampling strategy. The t-Lagrangian statistics are obtained from the velocity series sampled isochrone along trajectories, the s-Lagrangian statistics from equidistant sampling.

t-Lagrangian velocity series exhibit intermittent patterns characterized by long periods of low velocities and short high frequency fluctuations of high velocities. Intermittency is also reflected in the evolution of the t-Lagrangian velocity PDFs in that they are characterized by slow convergence at the low velocity end of the PDF. Particles at low velocities remain there for a long time, which is given by the advective travel time, or, in other words, particles have long memory of low velocities. For particles to become statistically equal, they all need to have access to the same statistics, This is possible only for times larger than the largest memory scale, which in turn is related to the distribution of the smallest velocities. Thus, the temporal evolution of particle velocities is characterized by history dependent dynamics.

This is different for the s-Lagrangian velocities, which do not display intermittent behavior. They evolve on a characteristic correlation length scale. This implies that particles become statistically equal, this means (spatial) memory is wiped out at distances larger than the correlation scale. We expect these behaviors to hold in 3-dimensional porous media as well because the fundamental mechanism, namely the variability of particle velocities on characteristics length scales imprinted in the medium, is the same. This is confirmed by preliminary results for 3-dimensional heterogeneous media. From a quantitative viewpoint, we expect differences in the correlation length and streamline tortuosity due to the additional spatial dimension, which may accelerate the convergence of the s-Lagrangian statistics toward steady state.

Quantifying the relatively simpler dynamics of s-Lagrangian velocities allows to understand and quantify the more complex intermittent dynamics of the velocity time series. We model the evolution of the s-Lagrangian velocity series in terms of a stationary and ergodic Markov processes based on the existence of a single relaxation length scale, the velocity correlation scale. The Markov process is parameterized in terms of the steady state s-Lagrangian velocity PDF $p_s(v)$ and the characteristic length scale ℓ_c . A key result relates the transport attribute $p_s(v)$ to the flow attribute $p_e(v)$, the Eulerian velocity PDF, by flux-weighting. The Eulerian velocity PDF can be obtained by spatial sampling, this means independently from a transport measurement. These results are valid for 2- and 3-dimensional heterogeneous porous media. The Markov approach is able to predict the evolution of particle velocities along streamlines for arbitrary initial conditions and can be conditioned on the heterogeneity distribution at the injection point. In this sense it is able to account for local scale information in a global upscaled model.

This Markov approach for the s-Lagrangian velocities places particle motion in the framework of time-domain and continuous time random walks [*Berkowitz et al.*, 2006; *Fiori et al.*, 2007] in that particles make transitions over a fixed spatial distances with an associated variable transition time. Particle motion along the x -axis may be described by

$$\frac{dx}{ds} = \chi^{-1}, \quad \frac{dt}{ds} = \frac{1}{v_s(s)}, \quad (51)$$

where χ is the advective tortuosity, which compares the average streamline length to the linear distance. Tortuosity accounts for the fact that the streamlines length s is in general larger than the linear distance. Note that in general, local tortuosity, this means the ratio of streamline length to linear distance, is different for each streamline. However, for ergodic media, we expect the average χ to be a good predictor for linear travel distances larger than ℓ_c . These points and the expression of χ in terms of the Eulerian flow statistics along the lines of *Koponen et al.* [1996] is discussed in a forthcoming paper.

We discuss two Markov models for the s-Lagrangian velocity series of different complexity. An Ornstein-Uhlenbeck process for the normal scores of velocity and a Bernoulli process for $v_s(s)$. While the Ornstein-Uhlenbeck process provides accurate predictions for the full evolution of the velocity statistics, the Bernoulli model captures the evolution only qualitatively. Still, the Bernoulli model is appealing due to its simplicity, which

allows to obtain analytical expressions for large scale dispersion. Specifically, the asymptotic large scale dispersion coefficient reads as [Dentz *et al.*, 2016],

$$D_L^* = \frac{\langle v_e \rangle^2 \ell_c}{\chi^2} \int_0^\infty dv p_e(v) \frac{\langle v_e \rangle - v}{v \langle v_e \rangle}, \quad (52)$$

if it exists. For the lognormal conductivity distribution it does exist. Note that for weak heterogeneity, this means $\sigma_f^2 < 1$, $p_e(v) \sim p_K(k)$ follows also a lognormal distribution, $\chi \approx 1$ and $\ell_c \approx \lambda$. In this case, expression (52) reduces to (1). Solute and particle transport in this framework is studied in detail in a forthcoming paper.

The proposed s-Lagrangian Markov approach is predictive in that it can be parameterized by the Eulerian velocity PDF, a flow attribute, and the correlation length of subsequent particle velocities. The latter is found to be model and heterogeneity dependent, but in any case of the order of the correlation length of the hydraulic conductivity field. We find that ℓ_c increases with increasing heterogeneity. In fact, it grows linearly with the variance of the logarithm of K . Also, the Eulerian velocity PDF can be represented over certain ranges by the PDF of hydraulic conductivity. However, further research is needed to arrive at a more quantitative theoretical understanding of the relations between the hydraulic conductivity distribution and structure, and the velocity correlation length and Eulerian flow statistics.

Acknowledgments

The authors thank Tanguy Le Borgne and Vladimir Cvetkovic for stimulating discussions. The authors acknowledge the support of the European Research Council (ERC) through the project MHetScale (contract number 617511). The data presented in this study is based on numerical simulations of flow and particle transport in synthetic media and numerical solutions of the presented stochastic models. All the data can be generated by following the steps detailed in the paper.

A: Flow statistics in Lognormal hydraulic conductivity fields

The section provides details on the validation of the numerical flow simulations for Lognormal hydraulic conductivity field against published results on the statistics of the Eulerian velocity field.

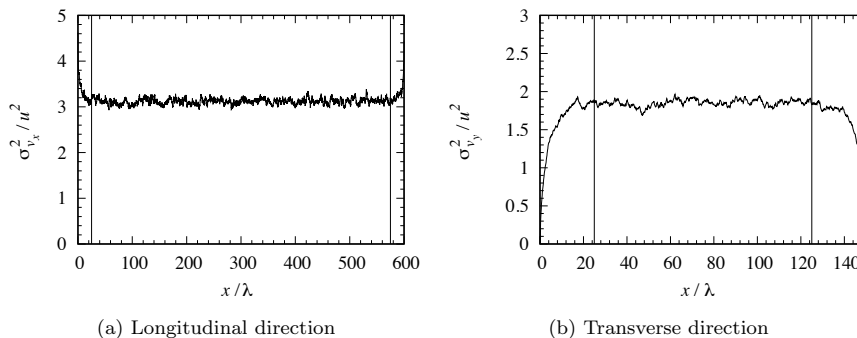


Figure A.1: Variance of Eulerian velocity for the Lognormal K field with $\sigma_f^2 = 7$. The vertical lines indicate the boundaries of the stationary domain used for particle tracking simulations.

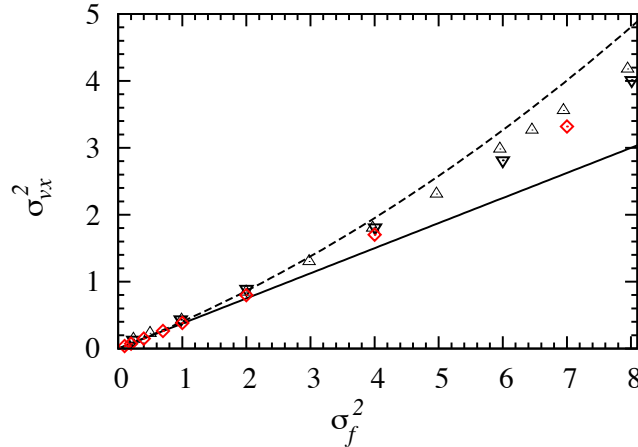


Figure B.1: Variance of the velocity component along the mean flow direction for Lognormally distributed K fields. Our simulations (red diamond) agrees with references from the literature: upward triangles from *de Dreuzy et al.* [2007b] and downward triangles from *Gotovac et al.* [2009].

A.1 Sub-domain size determination

To compute flow statistics and perform particle tracking in flow fields with steady statistics, it is required to estimate the width of a biased belt. Figure: A.1) shows the evolution of the variance in the directions longitudinal and transverse to the mean flow direction for the log-hydraulic conductivity field following a Lognormal distribution with the highest variance considered in this study ($\sigma_f^2 = 7$). Steady statistics are obtained in both directions within a belt of 20 correlation length. In a conservative way, this belt width was used for all fields with lower variance.

A.2 Variance of the flow field

To assess the accuracy of our numerical simulations, we compared the dependence of the variance of the velocity component longitudinal to the mean flow direction on the increase of σ_f^2 to (1) first and second order perturbation theory and (2) numerical results from the literature [*de Dreuzy et al.*, 2007b; *Gotovac et al.*, 2009]. Figure B.1 shows the variance of the Eulerian velocity along the mean flow direction as a function of σ_f^2 as well as the first- and second order perturbation theory solutions. Our results are in very good agreement with the references data from the literature, thus confirming the accuracy of our flow simulations.

B: Parameter estimation in the Ornstein-Uhlenbeck process

This section describes the procedure to estimate the velocity correlation parameter ℓ_c of the Ornstein-Uhlenbeck (OU) model. This estimation uses the map of the evolution of the space-Lagrangian velocity process to the w process. On average, the mean s-Lagrangian velocity relaxes to the flux-weighted mean of the Eulerian velocity field. This flux-weighted Eulerian mean is mapped to steady-state mean of the w process, which is $\mu = 0$. While the evolution of the mean velocity can be computed numerically, it is convenient to estimate the correlation value ℓ_c with the w process, because the latter can be described analytical. In short, we estimate the value of ℓ_c by fitting the analytical solution that describes the evolution of the mean of the Gaussian random variable w in the Ornstein-Uhlenbeck model.

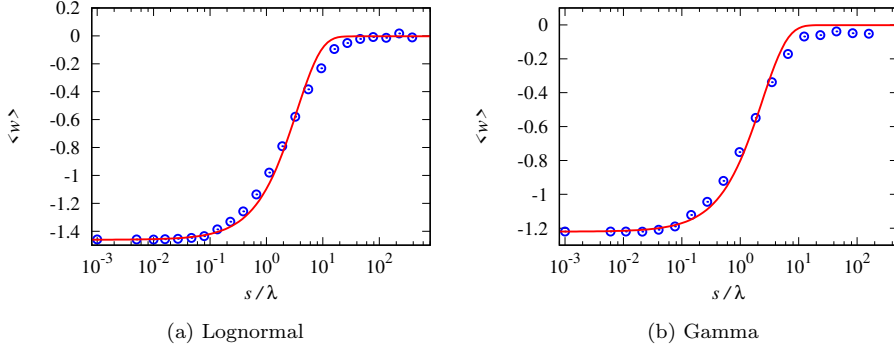


Figure B.2: Spatial evolution of the mean of the w process obtained by direct numerical simulations (blue signs) and with the fitted analytical solution (red line). Left: point K distribution is Lognormal, with $\sigma_Y^2 = 7$. Right: point K distribution is the Gamma, with $\sigma_f^2 = 4.9$ (i.e. $\alpha = 1/2$). The fitted correlation lengths are $\ell_c = 3.5$ and $\ell_c = 2.2$ for the Lognormal and Gamma K distributions respectively.

In the OU-model, the evolution of the mean for a unit Gaussian distribution is given by [Gardiner, 1985]

$$\langle w(s) \rangle = (\langle w_0 \rangle - \mu) \exp(-s/\ell_c) + \langle w_\infty \rangle, \quad (\text{B.1})$$

where $\langle w_0 \rangle$ and $\langle w_\infty \rangle$ are the initial and steady-state mean of $w(s)$. Figure B.2 shows an example of the spatial evolution of the empirical ensemble mean w process ($\langle w \rangle$) that stems from direct numerical simulations of transport in heterogeneous Lognormal and Gamma K fields. In addition, the figure shows the fitted analytical solution (Equation B.1) for mean value of the Gaussian variable in the OU process. The analytical solution gives satisfactory results and plots over the empirical data.

References

- Bear, J. (1972), *Dynamics of Fluids in Porous Media*, American Elsevier, New York.
- Beaudoin, A., and J.-R. de Dreuzy (2013), Numerical assessment of 3-d macrodispersion in heterogeneous porous media, *Water Resources Research*, *49*(5), 2489–2496, doi:10.1002/wrcr.20206.
- Bellin, A., P. Salandin, and A. Rinaldo (1992), Simulation of dispersion in heterogeneous porous formations: Statistics, first-order theories, convergence of computations, *Water Resources Research*, *28*(9), 2211–2227, doi:10.1029/92wr00578.
- Benke, R., and S. Painter (2003), Modeling conservative tracer transport in fracture networks with a hybrid approach based on the boltzmann transport equation, *Water Resources Research*, *39*, 1324, doi:10.1029/2003WR001966.
- Benson, D. A., S. W. Wheatcraft, and M. M. Meerschaert (2000), Application of a fractional advection-dispersion equation, *Water Resources Research*, *36*(6), 1403–1412, doi:10.1029/2000WR900031.
- Berkowitz, B., and H. Scher (1997), Anomalous transport in random fracture networks, *Physical Review Letters*, *79*(20), 4038–4041.
- Berkowitz, B., A. Cortis, M. Dentz, and H. Scher (2006), Modeling non-fickian transport in geological formations as a continuous time random walk, *Reviews of Geophysics*, *44*(2).
- Carrera, J., X. Sánchez-Vila, I. Benet, A. Medina, G. Galarza, and J. Guimerà (1998), On matrix diffusion: formulations, solution methods and qualitative ef-

- fects, *Hydrogeology Journal*, 6(1), 178–190.
- Comolli, A., and M. Dentz (2017), Anomalous dispersion in correlated porous media: a coupled continuous time random walk approach, *The European Physical Journal B*, 90(9), 166.
- Cushman, J. H., and T. R. Ginn (2000), Fractional advection-dispersion equation: a classical mass balance with convolution-fickian flux, *Water Resources Research*, 36(12), 3763–3766.
- Cushman, J. H., X. Hu, and T. R. Ginn (1994), Nonequilibrium statistical mechanics of preasymptotic dispersion, *Journal of Statistical Physics*, 75(5-6), 859–878, doi:10.1007/bf02186747.
- Cushman, J. H., L. S. Bennethum, and B. X. Hu (2002), A primer on upscaling tools for porous media, *Advances in Water Resources*, 25(8-12), 1043–1067, doi:10.1016/s0309-1708(02)00047-7.
- Cvetkovic, V., G. Dagan, and A. Shapiro (1991), An exact solution of solute transport by one-dimensional random velocity fields, *Stochastic Hydrology and Hydraulics*, 5(1), 45–54.
- Cvetkovic, V., H. Cheng, and X.-H. Wen (1996), Analysis of nonlinear effects on tracer migration in heterogeneous aquifers using Lagrangian travel time statistics, *Water Resources Research*, 32(6), 1671–1680.
- Cvetkovic, V., A. Fiori, and G. Dagan (2014), Solute transport in aquifers of arbitrary variability: A time-domain random walk formulation, *Water Resources Research*, 50(7), 5759–5773.
- Dagan, G. (1984), Solute transport in heterogeneous porous formations, *Journal of fluid mechanics*, 145, 151–177.
- Dagan, G. (1989), *Flow and Transport in Porous Formations*, Springer Nature, doi:10.1007/978-3-642-75015-1.
- Dagan, G. (2017), Solute plumes mean velocity in aquifer transport: Impact of injection and detection modes, *Advances in Water Resources*, 106, 6–10.
- Darcy, H. (1856), *Les fontaines publiques de la ville de Dijon*, V. Dalmont.
- De Anna, P., T. Le Borgne, M. Dentz, A. M. Tartakovsky, D. Bolster, and P. Davy (2013), Flow intermittency, dispersion, and correlated continuous time random walks in porous media, *Physical Review Letters*, 110(18), 184,502.
- de Dreuzy, J.-R., A. Beaudoin, and J. Erhel (2007a), Asymptotic dispersion in 2d heterogeneous porous media determined by parallel numerical simulations, *Water Resources Research*, 43(10), doi:10.1029/2006wr005394.
- de Dreuzy, J.-R., A. Beaudoin, and J. Erhel (2007b), Asymptotic dispersion in 2D heterogeneous porous media determined by parallel numerical simulations, *Water Resources Research*, 43(10), doi:10.1029/2006wr005394.
- De Marsily, G. (1986), *Quantitative hydrogeology: groundwater hydrology for engineers*, vol. 440, Academic Press San Diego, California.
- De Marsily, G., E. Ledoux, A. Barbreau, and J. Margat (1977), Nuclear waste disposal: can the geologist guarantee isolation?, *Science*, 197(4303), 519–527.
- Demmy, G., S. Berglund, and W. Graham (1999), Injection mode implications for solute transport in porous media: Analysis in a stochastic lagrangian framework, *Water Resources Research*, 35(7), 1965–1973, doi:10.1029/1999wr900027.
- Dentz, M., and B. Berkowitz (2003), Transport behavior of a passive solute in continuous time random walks and multirate mass transfer, *Water Resources Research*, 39(5), doi:10.1029/2001wr001163.
- Dentz, M., P. K. Kang, A. Comolli, T. L. Borgne, and D. R. Lester (2016), Continuous time random walks for the evolution of lagrangian velocities, *Physical Review Fluids*, 1(7), doi:10.1103/physrevfluids.1.074004.
- Domenico, P. A., and F. W. Schwartz (Eds.) (1997), *Physical and Chemical Hydrogeology*, Wiley.

- Eames, I., and J. W. M. Bush (1999), Longitudinal dispersion by bodies fixed in a potential flow, *Proceedings of the Royal Society A: Mathematical, Physical and Engineering Sciences*, 455(1990), 3665–3686, doi:10.1098/rspa.1999.0471.
- Ederly, Y., A. Guadagnini, H. Scher, and B. Berkowitz (2014), Origins of anomalous transport in heterogeneous media: Structural and dynamic controls, *Water Resources Research*, 50(2), 1490–1505.
- Eftekhari, A. A. (2015), FVTool: a finite volume toolbox for Matlab, doi: 10.5281/zenodo.18156.
- Fiori, A., I. Janković, and G. Dagan (2003), Flow and transport in highly heterogeneous formations: 2. semianalytical results for isotropic media, *Water Resources Research*, 39(9), doi:10.1029/2002wr001719.
- Fiori, A., I. Janković, and G. Dagan (2006), Modeling flow and transport in highly heterogeneous three-dimensional aquifers: Ergodicity, Gaussianity, and anomalous behavior-2. approximate semianalytical solution, *Water Resources Research*, 42(6), doi:10.1029/2005wr004752.
- Fiori, A., I. Janković, G. Dagan, and V. Cvetković (2007), Ergodic transport through aquifers of non-gaussian log conductivity distribution and occurrence of anomalous behavior, *Water resources research*, 43(9).
- Fogg, G. E. (2010), Log-k variance, connectivity, unconformities and non-fickian transport, in *2010 GSA Denver Annual Meeting*.
- Freeze, R. A., and J. A. Cherry (Eds.) (1979), *Groundwater*, Prentice Hall.
- Galassi, M., J. Davies, J. Theiler, B. Gough, G. Jungman, P. Alken, M. Booth, F. Rossi, and R. Ulerich (2016), *GNU Scientific Library Reference Manual*, Network Theory Ltd.
- Gardiner, C. (1985), Stochastic methods, *Springer Series in Synergetics (Springer-Verlag, Berlin, 2009)*.
- Gelhar, L. (1993), *Stochastic Subsurface Hydrology*, Prentice-Hall.
- Gelhar, L. W., and C. L. Axness (1983), Three-dimensional stochastic analysis of macrodispersion in aquifers, *Water Resources Research*, 19(1), 161–180, doi: 10.1029/wr019i001p00161.
- Gotovac, H., V. Cvetkovic, and R. Andricevic (2009), Flow and travel time statistics in highly heterogeneous porous media, *Water Resources Research*, 45(7), doi:10.1029/2008wr007168.
- Haggerty, R., and S. M. Gorelick (1995), Multiple-rate mass transfer for modeling diffusion and surface reactions in media with pore-scale heterogeneity, *Water Resources Research*, 31(10), 2383–2400.
- Haslauer, C., P. Guthke, A. Bárdossy, and E. Sudicky (2012), Effects of non-gaussian copula-based hydraulic conductivity fields on macrodispersion, *Water Resources Research*, 48(7).
- Hyman, J. D., S. L. Painter, H. Viswanathan, N. Makedonska, and S. Karra (2015), Influence of injection mode on transport properties in kilometer-scale three-dimensional discrete fracture networks, *Water Resources Research*, 51(9), 7289–7308.
- Kang, P. K., M. Dentz, T. Le Borgne, and R. Juanes (2011), Spatial markov model of anomalous transport through random lattice networks, *Physical Review Letters*, 107, 180,602.
- Kang, P. K., P. de Anna, J. P. Nunes, B. Bijeljic, M. J. Blunt, and R. Juanes (2014), Pore-scale intermittent velocity structure underpinning anomalous transport through 3-D porous media, *Geophysical Research Letters*, 41(17), 6184–6190, doi:10.1002/2014gl061475.
- Kang, P. K., M. Dentz, T. Le Borgne, S. Lee, and R. Juanes (2017), Anomalous transport in disordered fracture networks: spatial markov model for dispersion with variable injection modes, *Advances in Water Resources*.

- Koponen, A., M. Kataja, and J. Timonen (1996), Tortuous flow in porous media, *Physical Review E*, 54(1), 406.
- Kubo, R., M. Toda, and N. Hashitsume (1991), *Statistical Physics II, Non-Equilibrium Statistical Mechanics*, Springer Verlag Berlin Heidelberg.
- Le Borgne, T., J.-R. de Dreuzy, P. Davy, and O. Bour (2007), Characterization of the velocity field organization in heterogeneous media by conditional correlation, *Water Resources Research*, 43(2), doi:10.1029/2006wr004875.
- Le Borgne, T., M. Dentz, and J. Carrera (2008a), Lagrangian statistical model for transport in highly heterogeneous velocity fields, *Physical Review Letters*, 101(9), 090,601.
- Le Borgne, T., M. Dentz, and J. Carrera (2008b), Spatial markov processes for modeling lagrangian particle dynamics in heterogeneous porous media, *Physical Review E*, 78(2), 026,308.
- Levy, M., and B. Berkowitz (2003), Measurement and analysis of non-fickian dispersion in heterogeneous porous media, *Journal of Contaminant Hydrology*, 64(3-4), 203–226.
- Lumley, J. (1962), The mathematical nature of the problem of relating lagrangian and eulerian statistical functions in turbulence, *Mécanique de la Turbulence*, (108), 17–26.
- Massoudieh, A., M. Dentz, and J. Alikhani (2017), A spatial markov model for the evolution of the joint distribution of groundwater age, arrival time, and velocity in heterogeneous media, *Water Resources Research*.
- Matheron, G. (1967), *Éléments pour une théorie des milieux poreux*, Masson et Cie.
- Meyer, D. W., and H. A. Tchelepi (2010), Particle-based transport model with Markovian velocity processes for tracer dispersion in highly heterogeneous porous media, *Water Resources Research*, 46(11), doi:10.1029/2009wr008925.
- Morales, V., M. Dentz, M. Willmann, and M. Holzner (2017), Stochastic dynamics of intermittent pore-scale particle motion in three-dimensional porous media: Experiments and theory, *Geophysical Research Letters*, 44(18), 9361–9371.
- Neuman, S. P., and D. M. Tartakovsky (2009), Perspective on theories of non-fickian transport in heterogeneous media, *Advances in Water Resources*, 32(5), 670–680.
- Neuman, S. P., and Y.-K. Zhang (1990), A quasi-linear theory of non-fickian and fickian subsurface dispersion: 1. theoretical analysis with application to isotropic media, *Water Resources Research*, 26(5), 887–902.
- Niemi, A., J. Bear, and J. Bensabat (Eds.) (2017), *Geological Storage of CO₂ in Deep Saline Formations*, Springer Netherlands.
- Noetinger, B., D. Roubinet, A. Russian, T. Le Borgne, F. Delay, M. Dentz, J.-R. de Dreuzy, and P. Gouze (2016), Random walk methods for modeling hydrodynamic transport in porous and fractured media from pore to reservoir scale, *Transport in Porous Media*, 115(2), 345–385.
- Painter, S. (1996), Evidence for non-Gaussian scaling behavior in heterogeneous sedimentary formations, *Water Resources Research*, 32(5), 1183–1195, doi: 10.1029/96wr00286.
- Painter, S., and V. Cvetkovic (2005), Upscaling discrete fracture network simulations: An alternative to continuum transport models, *Water Resources Research*, 41, W02,002, doi:10.1029/2004WR003682.
- Poinssot, C., and H. Geckeis (Eds.) (2012), *Radionuclide Behaviour in the Natural Environment*, Woodhead Publishing.
- Pollock, D. W. (1988), Semianalytical computation of path lines for finite-difference models, *Ground Water*, 26(6), 743–750, doi:10.1111/j.1745-6584.1988.tb00425.x.
- Pope, S. B. (2000), *Turbulent Flows*, Cambridge University Press.
- R Core Team (2015), *R: A Language and Environment for Statistical Computing*, R Foundation for Statistical Computing, Vienna, Austria.

- Rehfeldt, K. R., J. M. Boggs, and L. W. Gelhar (1992), Field study of dispersion in a heterogeneous aquifer: 3. geostatistical analysis of hydraulic conductivity, *Water Resources Research*, *28*(12), 3309–3324, doi:10.1029/92wr01758.
- Rubin, Y. (2003), *Applied stochastic hydrogeology*, Oxford University Press.
- Sanchez-Vila, X., A. Guadagnini, and J. Carrera (2006), Representative hydraulic conductivities in saturated groundwater flow, *Reviews of Geophysics*, *44*(3), n/a–n/a, doi:10.1029/2005RG000169.
- Schlather, M., A. Malinowski, P. J. Menck, M. Oesting, and K. Strokorb (2015), Analysis, simulation and prediction of multivariate random fields with package RandomFields, *Journal of Statistical Software*, *63*(8), doi:10.18637/jss.v063.i08.
- Schumer, R., D. A. Benson, M. M. Meerschaert, and B. Baeumer (2003), Fractal mobile/immobile solute transport, *Water Resources Research*, *39*(10), doi:10.1029/2003WR002141.
- Shapiro, A. M., and V. D. Cvetkovic (1988), Stochastic analysis of solute arrival time in heterogeneous porous media, *Water Resources Research*, *24*(10), 1711–1718.
- Sidle, R. C., B. Nilsson, M. Hansen, and J. Fredericia (1998), Spatially varying hydraulic and solute transport characteristics of a fractured till determined by field tracer tests, funen, denmark, *Water Resources Research*, *34*(10), 2515–2527.
- Taylor, G. I. (1921), Diffusion by continuous movements, *Proceedings of the london mathematical society*, *20*, 196–211.
- Tyukhova, A., M. Dentz, W. Kinzelbach, and M. Willmann (2016), Mechanisms of anomalous dispersion in flow through heterogeneous porous media, *Physical Review Fluids*, *1*(7), doi:10.1103/physrevfluids.1.074002.
- Zhang, Q. (1997), Multi-length-scale theories for scale-up problem and renormalized perturbation expansion, *Advances in Water Resources*, *20*(5-6), 317–333, doi:10.1016/s0309-1708(96)00048-6.